Tokyo Climate Center, Japan Meteorological Agency

TCC News

No. 30 Autumn 2012

Contents Page

El Niño Outlook (October 2012 – April 2013)

El Niño conditions, which had emerged in the Northern Hemisphere summer, weakened in the equatorial Pacific. The likelihood that El Niño conditions will last until the Northern Hemisphere winter or transition to ENSO neutral conditions during autumn and winter is equal.

El Niño/La Niña

In September 2012, the SST deviation in the NINO.3 region was +0.3°C. SSTs in most parts from the central equatorial Pacific to the eastern Pacific were above normal, but were closer to normal than in August (Figures 1 and 3a). Subsurface temperatures were above normal in the western equatorial Pacific. Those in the central part, which had been above normal in August, moved closer to normal, and below-normal temperatures were seen at depths of around 140 m (Figures 2 and 3b). In the atmosphere, convective activity was above normal over the western equatorial Pacific. Easterly winds in the lower troposphere were weaker than normal in the western part and stronger than normal in the central part.

According to JMA's El Niño prediction model, SSTs in the NINO.3 region will be mostly near normal during the prediction period (Figure 4). Taking prediction uncertainties into account, however, it remains possible that El Niño conditions will persist until the Northern Hemisphere winter. Considering all the above, the likelihood that El Niño conditions will last until the Northern Hemisphere winter or transition to ENSO neutral conditions during autumn and winter is considered to be equal.

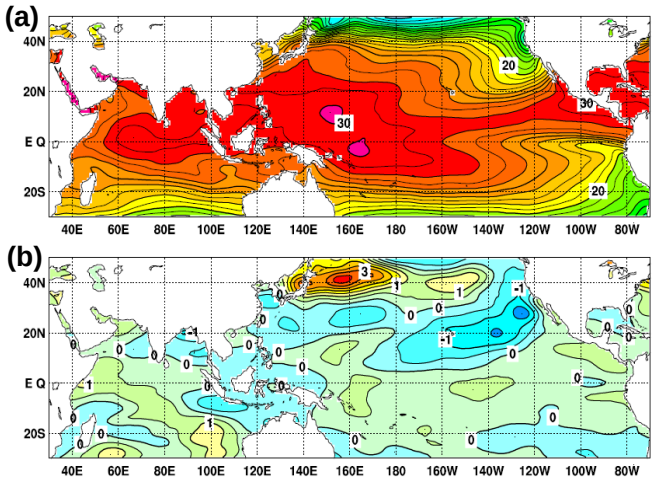

Figure 1 Monthly mean (a) sea surface temperatures (SSTs) and (b) SST anomalies in the Indian and Pacific Ocean areas for September 2012
The contour intervals are 1˚C in (a) and 0.5˚C in (b). The base period for the normal is 1981 – 2010.

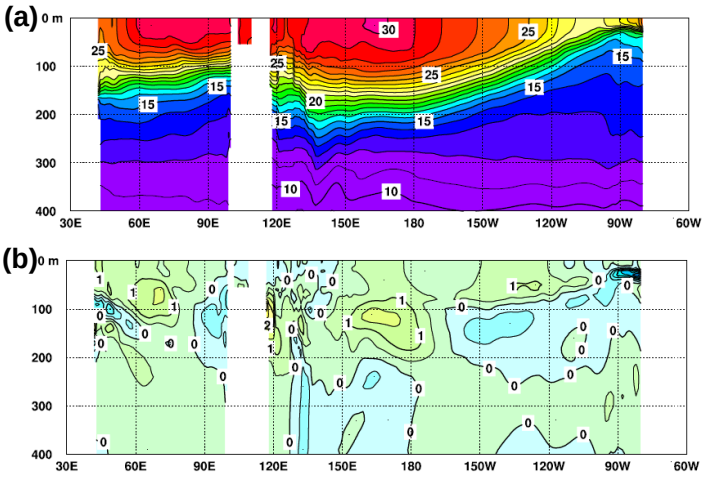

Figure 2 Monthly mean depth-longitude cross sections of (a) temperature and (b) temperature anomalies in the equatorial Indian and Pacific Ocean areas for September 2012
The contour intervals are 1˚C in (a) and 0.5˚C in (b). The base period for the normal is 1981 – 2010.

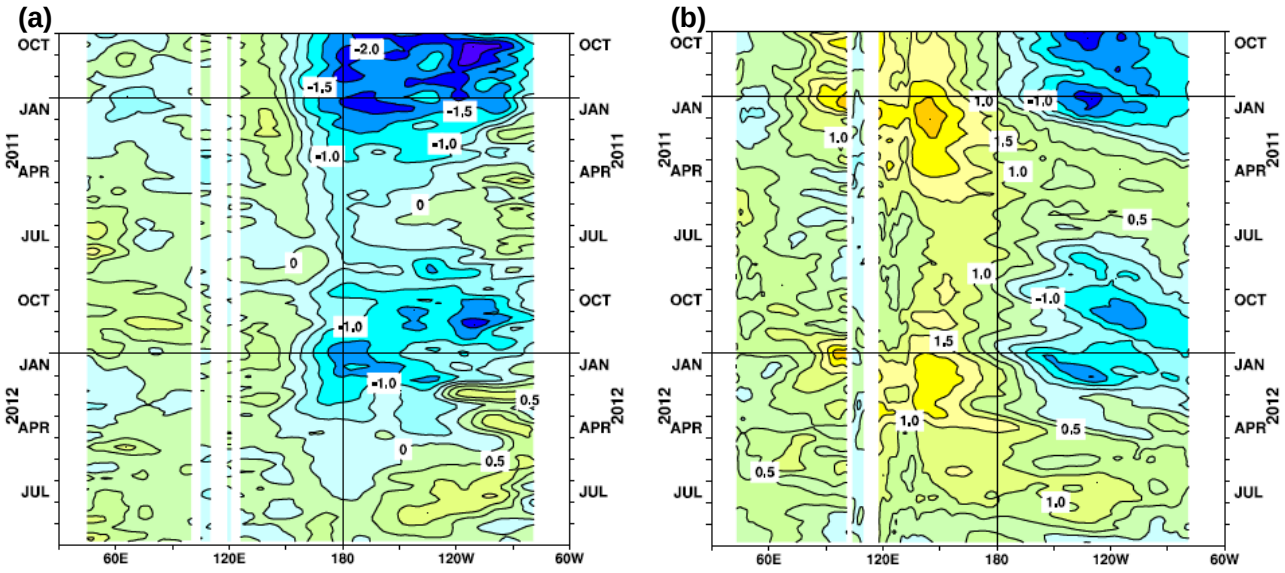

Figure 3 Time-longitude cross sections of (a) SST and (b) ocean heat content (OHC) anomalies along the equator in the Indian and Pacific Ocean areas

OHCs are defined here as vertical averaged temperatures in the top 300 m. The base period for the normal is 1981 – 2010.

Western Pacific and Indian Ocean

The area-averaged SST in the tropical western Pacific (NINO.WEST) region was below normal in September, and is likely to be near normal or below normal in the months ahead.

The area-averaged SST in the tropical Indian Ocean (IOBW) region was near normal in September, and is likely to be near normal in the months ahead.

(Ichiro Ishikawa, Climate Prediction Division)

* The SST normals for the NINO.WEST region (Eq. – 15°N, 130°E – 150°E) and the IOBW region (20°S – 20°N, 40°E – 100°E) are defined as linear extrapolations with respect to a sliding 30-year period in order to remove the effects of long-term trends.

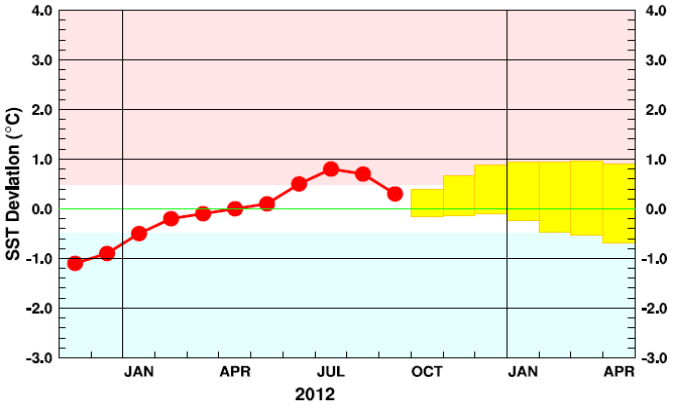

Figure 4 Outlook of NINO.3 SST deviation produced by the El Niño prediction model

This figure shows a time series of monthly NINO.3 SST deviations. The thick line with closed circles shows observed SST deviations, and the boxes show the values produced for the next six months by the El Niño prediction model. Each box denotes the range into which the SST deviation is expected to fall with a probability of 70%.

JMA's Seasonal Numerical Ensemble Prediction for Winter 2012/2013

According to JMA's seasonal ensemble prediction system, convection is expected to be active over the tropical Indian Ocean and the central equatorial Pacific and inactive around the Maritime Continent and east of the Philippines. In association with active convection over the tropical Indian Ocean, the sub-tropical jet stream is expected to shift northward over the western part of the Eurasian Continent and air temperatures are expected to be above normal around South Asia. Conversely, negative anomalies of air temperature are expected over the mid-latitudes of the Eurasian Continent.

1. Introduction

This article outlines JMA's dynamical seasonal ensemble prediction for winter 2012/2013 (December 2012 – February 2013, referred to as DJF), which was used as a basis for the Agency's operational cold-season outlook issued on 25 October, 2012. The outlook shown here is based on the seasonal ensemble prediction system of the Coupled atmosphere-ocean General Circulation Model (CGCM). See the column below for details of the system.

Section 2 outlines global SST anomaly predictions, and Section 3 describes the circulation fields expected over the tropics and sub-tropics in association with these anomalies. Finally, the circulation fields predicted for the mid- and high latitudes of the Northern Hemisphere are discussed in Section 4.

2. SST anomalies (Figure 5)

Figure 5 shows predicted SSTs and their anomalies for DJF. Above-normal values are expected in the central part of the equatorial Pacific and the tropical Indian Ocean.

3. Prediction for the tropics and sub-tropics (Figure 6)

Figure 6 (a) shows predicted precipitation and related anomalies for DJF. In association with the SST anomaly pattern over the equatorial Pacific, precipitation is expected to be above normal over the central equatorial Pacific and below normal around the Maritime Continent and east of the Philippines. From the tropical Indian Ocean to Southeast Asia, above-normal precipitation is expected. However, the results of hindcast experimentation indicate that the level of prediction skill for precipitation around Southeast Asia is relatively low. Accordingly, the prediction of above-normal levels over Southeast Asia and the related response to the large-scale atmospheric circulation detailed later should be interpreted with caution.

Velocity potential in the upper troposphere (200 hPa) (Figure 6 (b)) is expected to be negative (i.e., more divergent) over the tropical Indian Ocean and the central equatorial Pacific, reflecting active convection in these regions. Around the maritime continent, relatively positive (i.e., more convergent) anomalies are predicted, reflecting inactive convection.

The stream function at 200 hPa (Figure 6 (c)) is generally expected to be negative (i.e., cyclonic) in the mid-latitudes of the Northern Hemisphere, reflecting the zonal pattern of precipitation (i.e., active near the equator and inactive in the subtropics of the Northern Hemisphere). From South to Southeast Asia, positive (i.e., anti-cyclonic) anomalies are expected, reflecting active convection from the tropical Indian Ocean to Southeast Asia. In association with this, the sub-tropical jet stream is expected to shift northward over the western part of the Eurasian Continent and above-normal air temperatures are expected around South Asia (not shown). However, the prediction of these anomalies around Southeast Asia should be interpreted with caution because they may be affected by active convection over Southeast Asia, which is predicted with insufficient reliability.

Stream function anomalies at 850 hPa (Figure 6 (d)) are expected to be negative over the northern Indian Ocean in association with active convection in the region. Positive anomalies are predicted over the western tropical Pacific in association with inactive convection around the Maritime Continent and east of the Philippines.

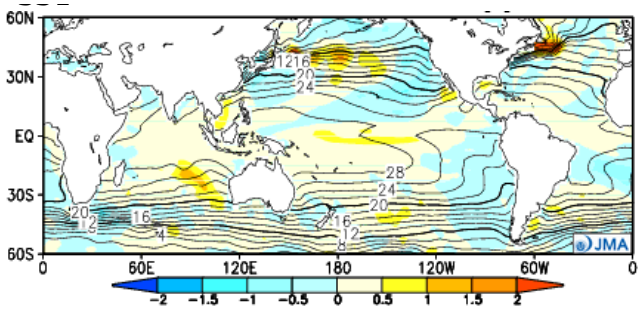

Figure 5 Predicted SSTs (contours) and SST anomalies (shading) for December 2012 – February 2013 (ensemble mean of 51 members)

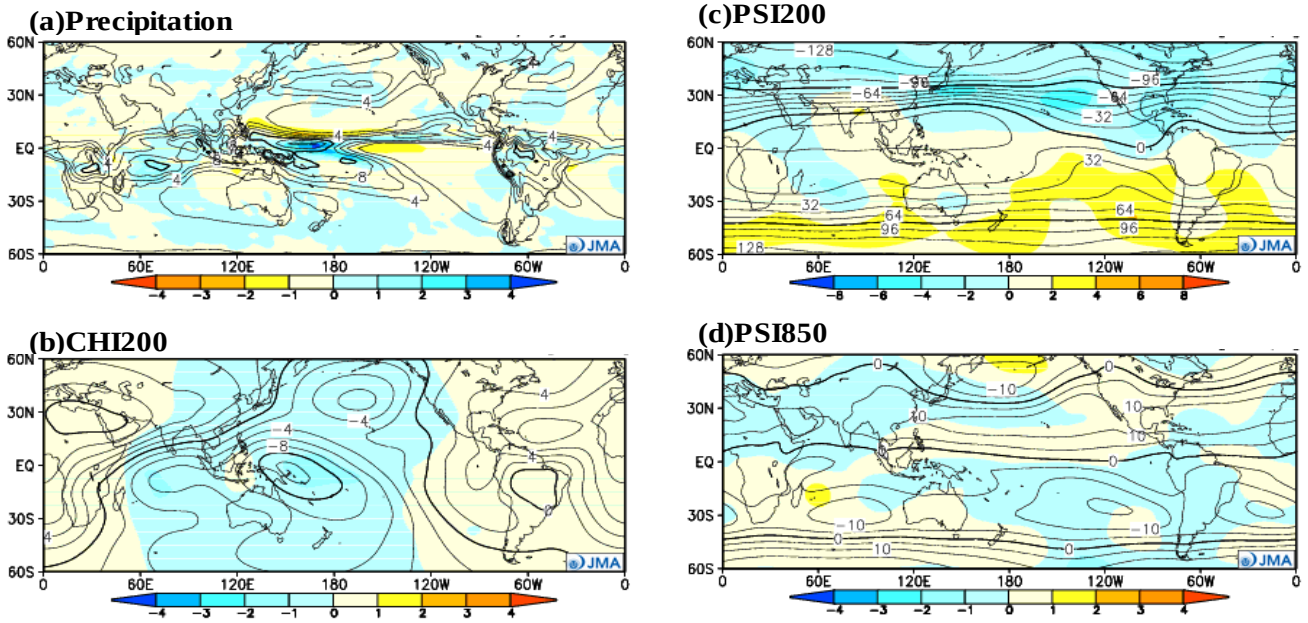

Figure 6 Predicted atmospheric fields from 60°N – 60°S for December 2012 – February 2013 (ensemble mean of 51 members)

(a) Precipitation (contours) and anomaly (shading). The contour interval is 2 mm/day.
(b) Velocity potential at 200 hPa (contours) and anomaly (shading). The contour interval is 2×10^6 m^2/s.
(c) Stream function at 200 hPa (contours) and anomaly (shading). The contour interval is 16×10^6 m^2/s.
(d) Stream function at 850 hPa (contours) and anomaly (shading). The contour interval is 5×10^6 m^2/s.

4. Prediction for the mid- and high latitudes of the Northern Hemisphere (Figure 7)

Around the Aleutian Low region, sea level pressure (SLP) anomalies (Figure 7(a)) are expected to be positive on the northern side and negative on the southern side, suggesting that the Aleutian Low will shift southward but its strength will be near normal. Conditions of the northwesterly winter monsoon are therefore expected to be near normal over East Asia. Negative anomalies of 500-hPa geopotential height (Figure 7(b)) are widely expected over the southern part of the Eurasian Continent, and this may be attributable to active convection covering the area from the tropical Indian Ocean to Southeast Asia. Accordingly, lower-atmospheric temperatures are expected to be below normal over the mid-latitudes of the Eurasian Continent (Figure 7(c)). However, the prediction of negative anomalies around East Asia should be interpreted with caution because they may be affected by active convection over Southeast Asia, which is predicted with insufficient reliability.

(Masayuki Hirai, Climate Prediction Division)

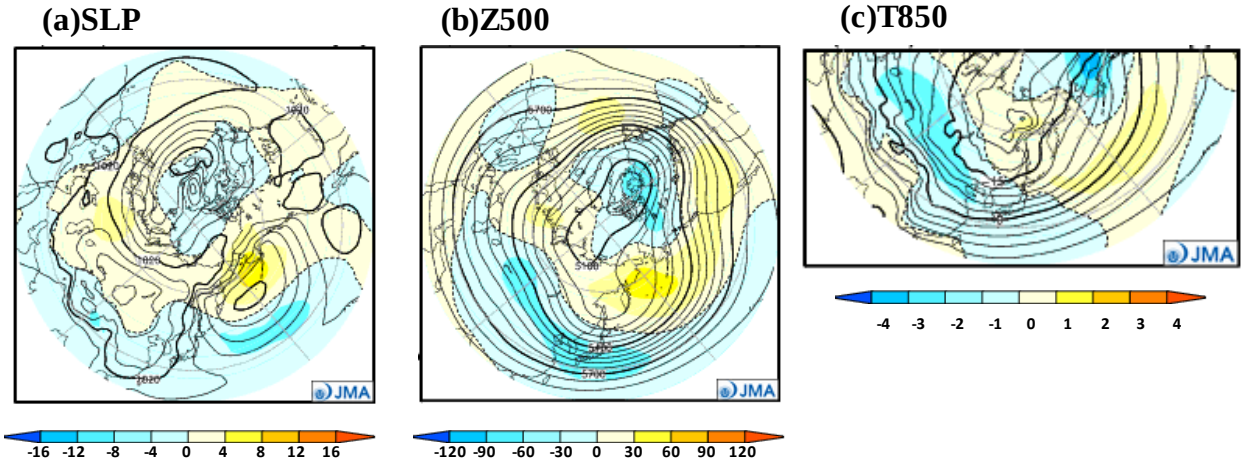

Figure 7 Predicted atmospheric fields from 20°N – 90°N for December 2012 – February 2013 (ensemble mean of 51 members)
(a) Sea level pressure (contours) and anomaly (shaded). The contour interval is 4 hPa.
(b) 500-hPa height (contours) and anomaly (shaded). The contour interval is 60 m.
(c) 850-hPa temperature (contours) and anomaly (shaded). The contour interval is 3˚C.

JMA's Seasonal Ensemble Prediction System

JMA operates a seasonal Ensemble Prediction System (EPS) using the Coupled atmosphere-ocean General Circulation Model (CGCM) to make seasonal predictions beyond a one-month time range. The EPS produces perturbed initial conditions by means of a combination of the initial perturbation method and the lagged average forecasting (LAF) method. The prediction consists of 51 members from the latest 6 initial dates (9 members are run every 5 days). Details of the prediction system and verification maps based on 30-year hindcast experiments (1979 – 2008) are available at http://ds.data.jma.go.jp/tcc/tcc/products/model/.

Cold Season Outlook for Winter 2012/2013 in Japan

For winter 2012/2013, mean temperatures are likely to be above or near normal in eastern Japan, western Japan and Okinawa/Amami. Cold-season precipitation amounts are likely to be above or near normal in Okinawa/Amami.

1. Outlook summary

JMA issued its outlook for the coming winter over Japan in September and updated it in October. For winter 2012/2013, mean temperatures are likely to be above or near normal in eastern Japan, western Japan and Okinawa/Amami with 40% probability for both categories (Figure 8). Cold season precipitation amounts are likely to be above or near normal in Okinawa/Amami with 40% probability for both categories (Figure 9).

Category	–	0	+
Northern Japan	30	40	30
Eastern Japan	20	40	40
Western Japan	20	40	40
Okinawa and Amami	20	40	40

Figure 8 Outlook for winter 2012/2013 temperature probability in Japan

2. Outlook background

JMA's coupled global circulation model predicts that the NINO.3 SST will be mostly near normal during the Northern Hemisphere autumn and winter. Taking prediction uncertainties into account, however, it remains possible that El Niño conditions will persist until winter. Considering all the above, the likelihood that El Niño conditions will last until winter or transition to ENSO neutral conditions during autumn and winter is equal.

In association with the SST anomaly pattern, some characteristics of the ensemble averaged atmospheric circulation anomaly pattern predicted by the model are similar to those of typical El Niño events in and around the tropics. For example, convection is expected to be inactive in the western tropical Pacific. In line with this, an anti-cyclonic circulation anomaly in the lower troposphere is predicted. There is a possibility that an anti-cyclonic circulation anomaly extending to the south of Japan will bring warm and humid air to the southern part of the country and create favorable conditions for cyclone genesis there.

Remarkable southward meandering of the jet stream over Japan is predicted in association with active convection around the Bay of Bengal. However, the model hindcast (30 years from 1979 to 2008) suggests that the model's skill is insufficient to predict convection around the Bay of Bengal. Moreover, the positive (negative) phase of the Arctic Oscillation (AO) tends to cause a weak (strong) winter monsoon and above-normal (below-normal) temperatures in northern Japan. However, the model results associated with the AO should be treated with caution because the spread of the AO index among ensemble members is large.

Considering the prediction skill of the model's results in the mid- and high-latitudes described above, it is most likely that El Niño characteristics will be observed around Japan in response to tropical conditions.

(Takafumi Umeda, Climate Prediction Division)

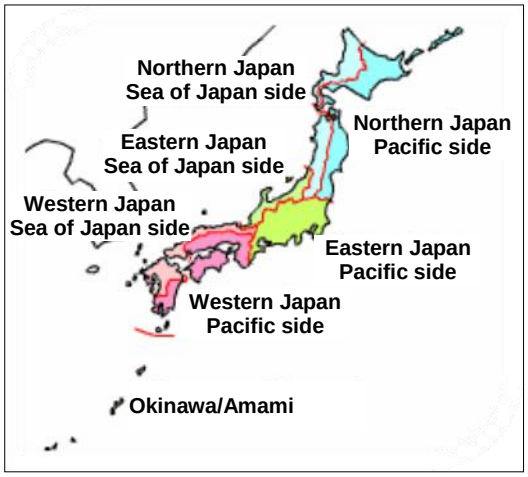

Category		–	0	+
Northern Japan	Sea of Japan side	30	40	30
	Pacific side	30	40	30
Eastern Japan	Sea of Japan side	40	30	30
	Pacific side	30	30	40
Western Japan	Sea of Japan side	30	40	30
	Pacific side	30	30	40
Okinawa and Amami		20	40	40

Figure 9 Outlook for winter 2012/2013 precipitation probability in Japan

Summary of the 2012 Asian Summer Monsoon

1. Precipitation and temperature

Four-month total precipitation amounts based on CLIMAT reports during the monsoon season (June – September) were above 200% of the normal around southern Pakistan, and were below 60% of the normal around Java Island (Figure 10). Values were mostly consistent with the distribution of OLR anomalies (Figure 12).

Extremely heavy precipitation was seen around Mongolia in June and July and over Pakistan in September. In contrast, extremely light precipitation was seen in western India in June and around western Indonesia in August (figures not shown).

Four-month mean temperatures for the same period were 1°C above the normal in northern Japan and from western Mongolia to northeastern India, and were 1°C below the normal from northeastern China to eastern

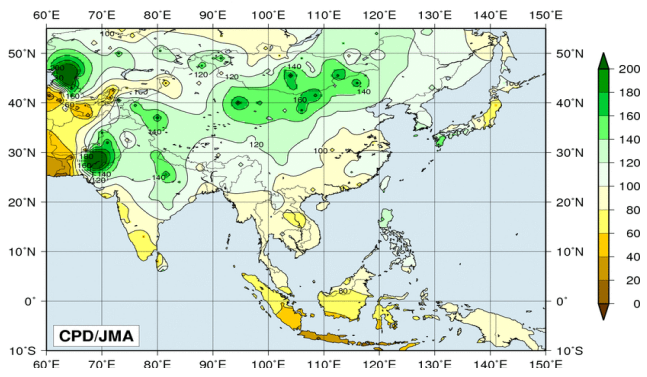

Figure 10 Four-month precipitation ratios (%) from June to September 2012
The base period for the normal is 1981 – 2010.

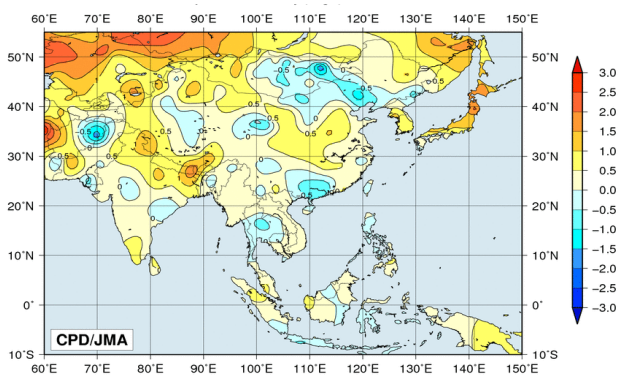

Figure 11 Four-month mean temperature anomalies (°C) from June to September 2012
The base period for the normal is 1981 – 2010.

Mongolia and in northern Pakistan (Figure 11).

It was reported that heavy rains caused more than 130 fatalities in Bangladesh and more than 120 fatalities in northern India's Assam region in June. It was also reported that heavy rains caused at least 100 fatalities in the Philippines due to typhoons and enhanced convective activity associated with monsoon in August. It was further reported that heavy rains from late August to September caused more than 450 fatalities in Pakistan.

2. Tropical cyclones

During the monsoon season, 16 tropical cyclones (TCs) of tropical storm (TS) intensity or higher formed over the western North Pacific (Table 1). The number of formations was the same as the 1981 – 2010 average of 16.0. A total of 8 among these 16 passed around the East China Sea and approached or hit China, the Korean Peninsula or Japan, while five approached or hit southern China or Viet Nam via the South China Sea. Two TCs hit the main islands of Japan.

Typhoon Saola caused more than 70 fatalities throughout China and the Philippines, and Typhoon Kai-tak caused more than 35 fatalities throughout the Philippines and Viet Nam.

Note: Disaster information is based on reports by governmental organizations (Bangladesh, China, India, Pakistan, the Philippines and Viet Nam).

3. Monsoon activity and atmospheric circulation

Convective activity (inferred from outgoing longwave radiation (OLR)) averaged for June – September 2012 was enhanced over the western Indian Ocean, Pakistan, northern India, the Bay of Bengal, the South China Sea and the tropical western Pacific, and was suppressed over western/southern India and the eastern Indian Ocean (Figure 12). According to the OLR indices (Table 2), convective activity averaged over the Bay of Bengal and in the vicinity of the Philippines (both core areas of monsoon-related active convection) was enhanced in the summer monsoon season except in August, and in particular, enhanced convective activity from the South China Sea to the area east of the Philippines persisted throughout the season (Figure 13). The large-scale active convection area of the monsoon showed a tendency to be shifted north and east of its normal position. The areas of active convection that were originally enhanced around the equatorial western Indian Ocean in the middle of August moved northward around India and reached Pakistan in early September (Figure 14 (a)).

Table 1 Tropical cyclones forming over the western North Pacific from June to September 2012

Number ID	Name	Date (UTC)	Category[1)]	Maximum wind[2)] (knots)
T1203	MAWAR	6/1 – 6/6	TY	75
T1204	GUCHOL	6/13 – 6/19	TY	100
T1205	TALIM	6/17 – 6/20	STS	50
T1206	DOKSURI	6/26 – 6/29	TS	40
T1207	KHANUN	7/16 – 7/18	STS	50
T1208	VICENTE	7/21 – 7/24	TY	80
T1209	SAOLA	7/28 – 8/3	TY	70
T1210	DAMREY	7/28 – 8/3	TY	70
T1211	HAIKUI	8/3 – 8/9	TY	65
T1212	KIROGI	8/6 – 8/10	STS	50
T1213	KAI-TAK	8/13 – 8/18	TY	65
T1214	TEMBIN	8/19 – 8/30	TY	80
T1215	BOLAVEN	8/20 – 8/29	TY	100
T1216	SANBA	9/11 – 9/17	TY	110
T1217	JELAWAT	9/20 – 10/1	TY	110
T1218	EWINIAR	9/24 – 9/29	STS	50

Note: Based on information from the RSMC Tokyo-Typhoon Center.
1) Intensity classification for tropical cyclones
TS: Tropical storm, STS: Severe tropical storm, TY: Typhoon
2) Estimated maximum 10-minute mean wind

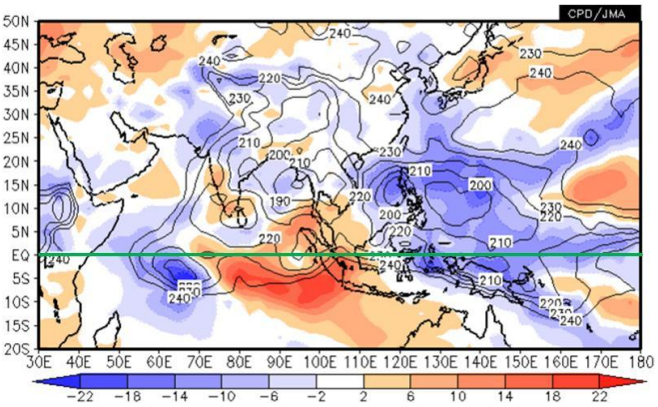

Figure 12 Four-month mean outgoing longwave radiation (OLR) and its anomaly for June – September 2012
The contours indicate OLR at intervals of 10 W/m^2, and the color shading denotes OLR anomalies from the normal (i.e., the 1981 – 2010 average). Negative (cold color) and positive (warm color) OLR anomalies show enhanced and suppressed convection compared to the normal, respectively. Original data provided by NOAA.

Table 2 Summer Asian Monsoon OLR Index (SAMOI) from May to October 2012
Asian summer monsoon OLR indices (SAMOI) are derived from OLR anomalies from May to October. SAMOI (A), (N) and (W) indicate the overall activity of the Asian summer monsoon, its northward shift and its westward shift, respectively. SAMOI definitions are as follows: SAMOI (A) = (–1) × (W + E); SAMOI (N) = S – N; SAMOI (W) = E – W. W, E, N and S indicate area-averaged OLR anomalies for the respective regions shown in the figure on the right normalized by their standard deviations.

	Summer Asian Monsoon OLR Index (SAMOI)		
	SAMOI (A): Activity	SAMOI (N): Northward-shift	SAMOI (W): Westward-shift
May 2012	0.7	-0.9	-0.8
Jun. 2012	0.7	1.2	-1.5
Jul. 2012	1.0	0.3	-1.4
Aug. 2012	-0.1	1.5	-1.0
Sep. 2012	1.6	0.2	0.2
Oct. 2012	-0.7	-1.2	-1.2

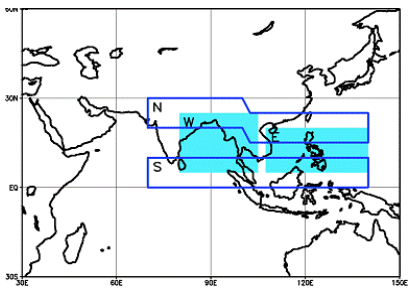

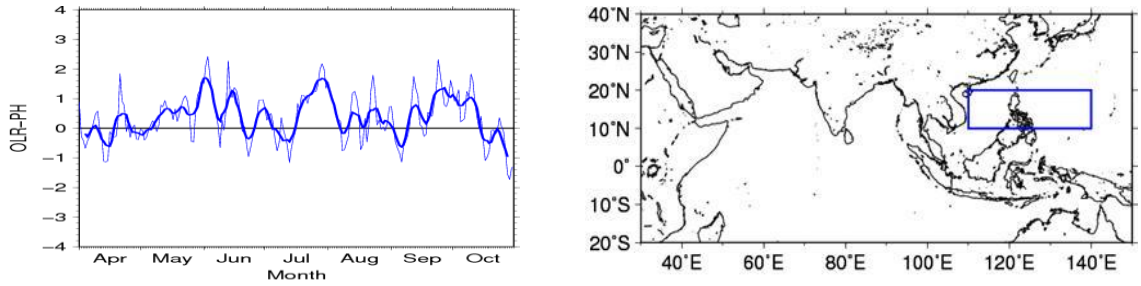

Figure 13 Time-series representation of the area-averaged OLR index (OLR-PH) around the Philippines (shown by the blue rectangle on the right: 10ºN – 20ºN, 110ºE – 140ºE)

The OLR index (OLR-PH) consists of reversed-sign area-averaged OLR anomalies for the area around the Philippines normalized by the standard deviation. Positive and negative OLR index values indicate enhanced and suppressed convective activity, respectively, compared to the normal (i.e., the 1981 – 2010 average). The thick and thin blue lines indicate seven-day running mean and daily mean values, respectively.

In the upper troposphere, the Tibetan High was pronounced around its central part (Figure 15 (a)). In the lower troposphere, a prominent monsoon trough stretching from the South China Sea to the Philippines was observed, and westerly winds were stronger than normal from the Bay of Bengal to the vicinity of the Philippines (Figure 15 (b)). Easterly vertical shear over the North Indian Ocean and southern Asia was stronger than normal (Figure 16). These characteristics of anomalous circulation indicate enhanced large-scale circulation related to the monsoon. The Pacific High in the lower troposphere was significantly enhanced to the east of Japan, bringing hot summer conditions to the country (Figure 15 (b)).

(1-2: Kazuyoshi Yoshimatsu, 3: Shotaro Tanaka, Climate Prediction Division)

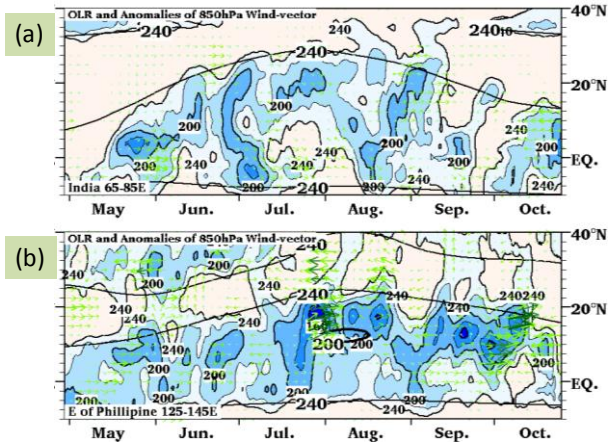

Figure 14 Latitude-time cross section of the five-day running mean OLR from May to October 2012 ((a) India (65ºE – 85ºE mean), (b) area east of the Philippines (125ºE – 145ºE mean))

The thick black lines indicate the climatological mean OLR (W/m^2) for the period from 1981 to 2010, and the shading denotes the OLR for 2012.

References

Webster, P. J., and S. Yang, 1992: Monsoon and ENSO: Selectively interactive systems. *Quart. J. Roy. Meteor. Soc.*, **118**, 877-926.

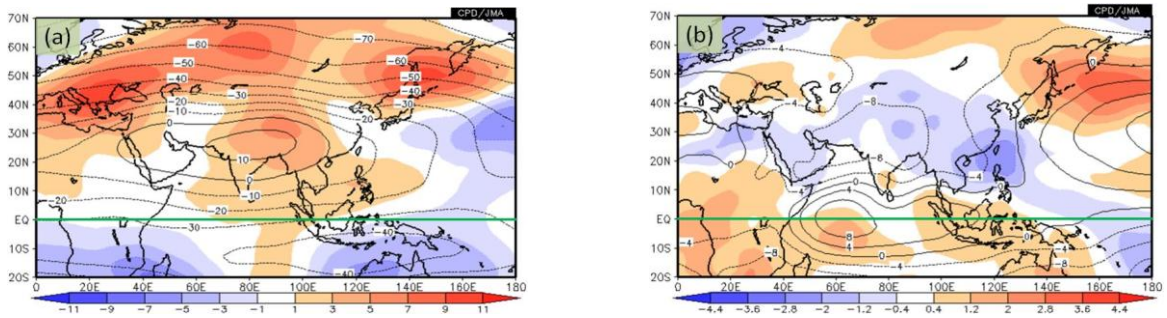

Figure 15 Four-month mean stream function and its anomaly for June – September 2012

(a) The contours indicate the 200-hPa stream function at intervals of 10×10^6 m^2/s, and the color shading indicates 200-hPa stream function anomalies from the normal. (b) The contours indicate the 850-hPa stream function at intervals of 4×10^6 m^2/s, and the color shading indicates 850-hPa stream function anomalies from the normal. The base period for the normal is 1981 – 2010. Warm (cold) shading denotes anticyclonic (cyclonic) circulation anomalies in the Northern Hemisphere, and vice versa in the Southern Hemisphere.

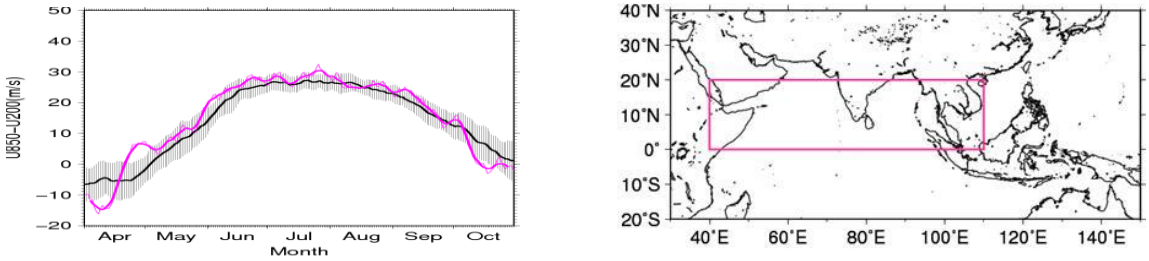

Figure 16 Time-series representation of the zonal wind shear index between 200 hPa and 850 hPa averaged over the North Indian Ocean and southern Asia (pink rectangle on the right: equator – 20ºN, 40ºE – 110ºE)

The zonal wind shear index is calculated after Webster and Yang (1992). The thick and thin pink lines indicate seven-day running mean and daily mean values, respectively. The black line denotes the normal (i.e., the 1981 – 2010 average), and the gray shading shows the range of the standard deviation calculated for the time period of the normal.

Extremely Hot Late-Summer Conditions in Northern and Eastern Japan in 2012

Northern and eastern Japan experienced extremely high temperatures in the late summer of 2012 due to the significantly enhanced North Pacific High to the east of the country. Record-high temperatures were set over northern Japan for three consecutive 10-day periods* from late August to mid-September. The 10-day mean sea surface temperature (SST) averaged over the area around northern Japan for mid-September was the highest on record for all 10-day periods of the year since 1985.

* Note: There are three 10-day periods in each month, making a total of thirty-six in a year. The third nominal 10-day period of each month may not in fact have only 10 days (e.g., the third 10-day period of August covers 11 days from the 21st to 31st).

1. Surface climate conditions

In northern and eastern Japan, hot sunny conditions prevailed from mid-August to mid-September, and temperatures remained significantly above normal for this time of the year (Figure 17). For example, Sapporo City in northern Japan's Hokkaido region experienced very hot conditions every day from late August to mid-September, and daily mean temperatures persisted above the annual high of the climatological normal (Figure 18).

The values of 10-day mean temperatures averaged over northern Japan were the highest on record for three consecutive 10-day periods from late August to mid-September (Table 3, top). Those for eastern Japan were the second highest on record for late August and early September, and the value for mid-September tied the record-high set in 2011 (Table 3, bottom). Collection of 10-day mean temperature records for divisions of Japan began in 1961.

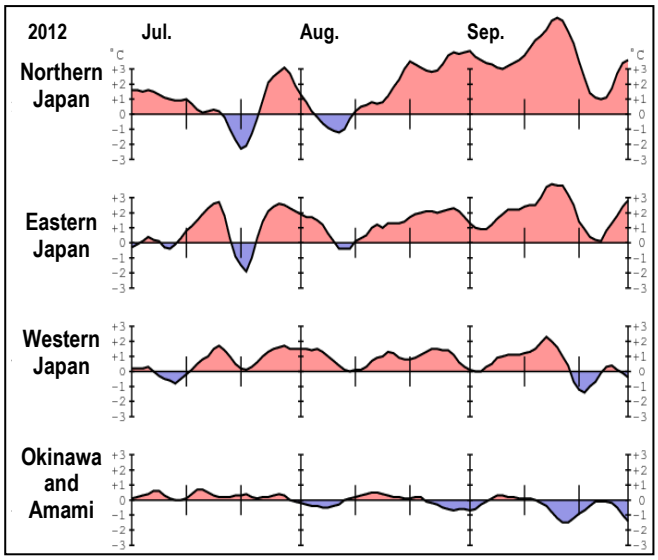

Figure 17 Time-series representation of five-day running mean temperature anomalies (unit: ˚C) for four divisions of Japan from 1 July to 30 September, 2012
Anomalies are deviations from the 1981 – 2010 average.

Table 3 Top three 10-day mean temperature anomalies (unit: ˚C) averaged over northern Japan (top) and eastern Japan (bottom) from late August to mid-September
Collection of statistical records began in 1961. Anomalies are deviations from the 1981 – 2010 average, and the figures in red denote records for 2012.

Northern Japan	Highest	2nd highest	3rd highest
21 – 31 August	**+3.5 (2012)**	+3.1 (2010)	+1.9 (2000)
1 – 10 September	**+3.3 (2012)**	+3.1 (2010)	+2.5 (2011)
11 – 20 September	**+5.5 (2012)**	+2.0 (2000)	+1.8 (2007)

Eastern Japan	Highest	2nd highest	3rd highest
21 – 31 August	+2.7 (2010)	**+2.1 (2012)**	+1.7 (2000)
1 – 10 September	+2.9 (2010)	**+1.5 (2012)**	+1.5 (1961)
11 – 20 September	**+3.1 (2012)**	+3.1 (2011)	+2.3 (2003)

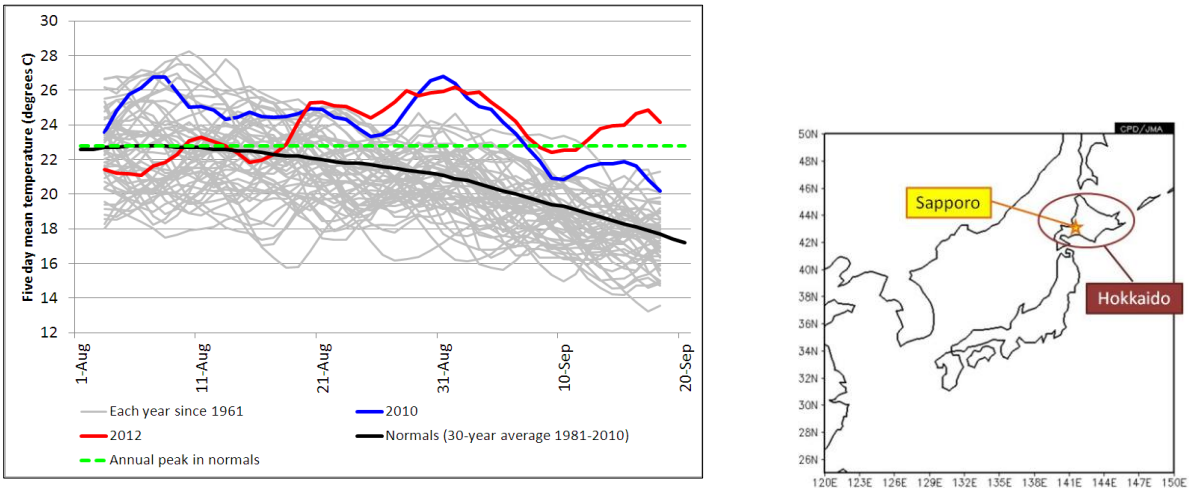

Figure 18 Time-series representation of five-day running mean temperatures in Sapporo from 3 August to 18 September between 1961 and 2012
The red and blue lines indicate values for 2012 and 2010 (the previous record for high temperatures in late summer), respectively. Green denotes the highest value among daily mean temperatures in the climatological normal (i.e., the 1981 – 2010 average) for Sapporo.

2. Characteristic atmospheric circulation causing Japan's hot late-summer conditions

The significantly enhanced Pacific High to the east of Japan persisted from late August to mid-September 2012 (Figures 19 and 20 (a)). Northern and eastern Japan experienced extremely high temperatures due to southerly warm-air advection and sunny conditions (i.e., above-normal amounts of solar radiation) attributed to the northward extension of this high.

The Pacific High to the east of Japan in late August – mid-September was at its strongest for this time of the year since 1979 (Figure 20 (b)). The westerly jet stream in the upper troposphere showed significant northward meandering near Japan (Figure 21) in line with prominent anticyclonic circulation anomalies centered over the area to the northeast of the country (Figure 22). In association, negative anomalies of potential vorticity (PV) in the upper troposphere were centered northeast of Japan (Figure 23).

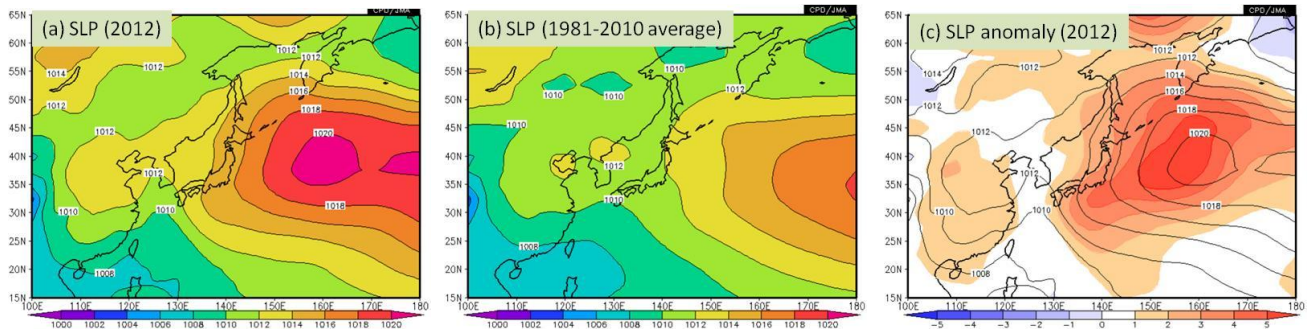

Figure 19 Sea level pressure (SLP) averaged from 21 August to 20 September for (a) 2012, (b) the normal (i.e., the 1981 – 2010 average) and (c) 2012 and anomalies (i.e., deviations from the normal)
The contour interval is 2 hPa.

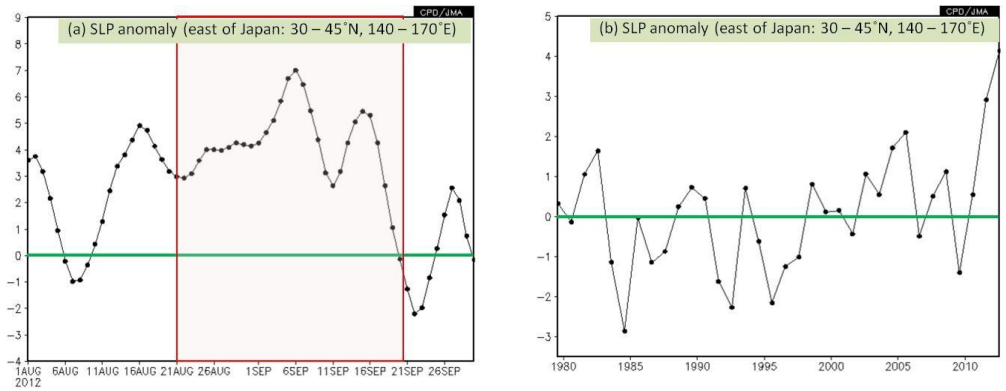

Figure 20 (a) Time-series representation of five-day running mean values of SLP anomalies (unit: hPa) averaged over the area east of Japan (30˚N – 45˚N, 140˚E – 170˚E) from 1 August to 30 September, 2012, and (b) interannual variability of area-mean SLP anomalies averaged between 21 August and 20 September from 1979 to 2012
Anomalies are deviations from the 1981 – 2010 average. The red rectangle in the panel on the left shows the period from 21 August to 20 September, 2012.

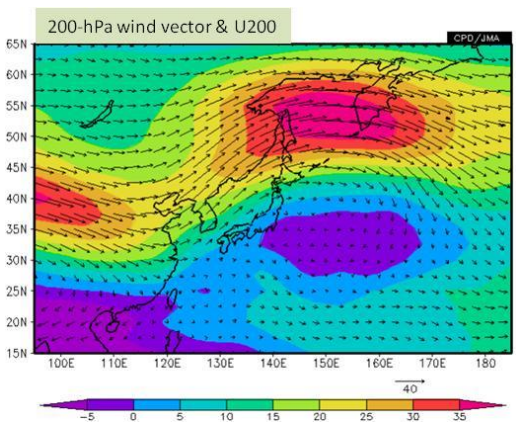

Figure 21 200-hPa wind vectors and zonal wind speeds averaged from 21 August to 20 September, 2012
The shading shows zonal wind speeds (unit: m/s).

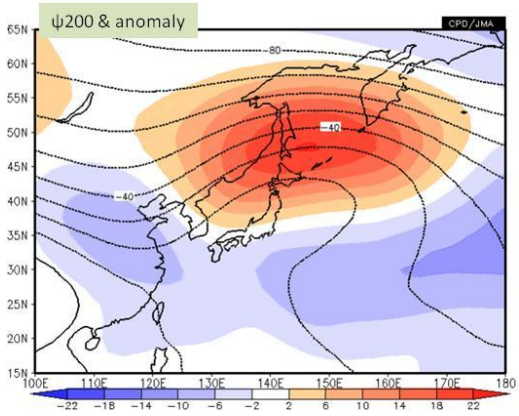

Figure 22 200-hPa stream function (contours) and anomalies (shading) averaged from 21 August to 20 September, 2012
The contour interval is 10^6 m^2/s. Positive (warm color) and negative (cold color) stream function anomalies in the Northern Hemisphere indicate anticyclonic and cyclonic circulation anomalies. Anomalies are deviations from the 1981 – 2010 average.

The enhanced anticyclone east of the country featured an equivalent barotropic structure and a warm air mass, and its vertical axis exhibited a slight northward tilt with height (Figure 24). It is presumed that upper-level PV anomalies induced the enhanced equivalent-barotropic anticyclone (Hoskins et al. 1985).

In the upper troposphere, wave trains were seen along the Asian jet stream in association with the eastward propagation of Rossby wave packets (Figure 25). Convective activity associated with the Asian summer monsoon was enhanced over the Arabian Sea, Pakistan, India and the Bay of Bengal (Figure 26). According to statistical analysis, when convective activity is enhanced over these areas in and around South Asia from late August to mid-September, wave trains with anticyclonic circulation anomalies north of Japan tend to appear along the Asian jet stream (Figure 27) as seen in 2012 (Figure 25). These trains are similar to those of the Silk Road pattern highlighted by T. Enomoto (Enomoto et al. 2003; Enomoto 2004). It can be presumed from the results of statistical analysis and research performed to date that active convection associated with monsoon activity in and around South Asia contributed to the development of the enhanced anticyclone near Japan through the eastward propagation of quasi-stationary Rossby wave packets along the Asian jet.

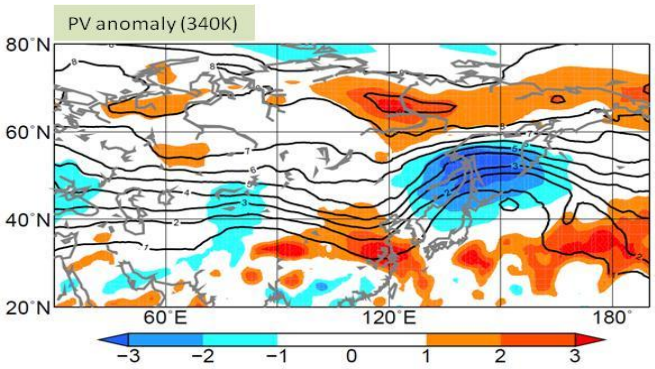

Figure 23 Potential vorticity on the 340 K isentropic surface (contours; unit: s^{-1}) and normalized anomalies (shading) averaged from 21 August to 20 September, 2012
Anomalies (i.e., deviations from the 1981 – 2010 average) are normalized by their standard deviations.

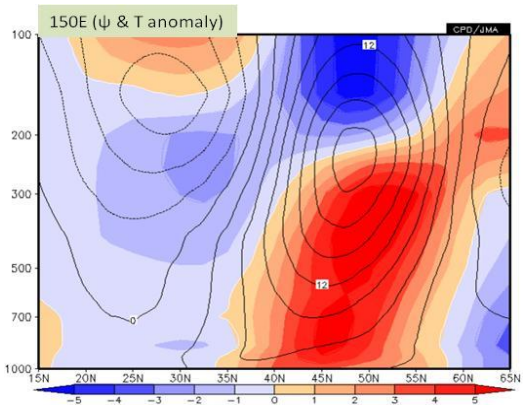

Figure 24 The vertical-meridional section of stream function anomalies (contours; unit: 10^6 m^2/s) and temperature anomalies (shading; unit: ˚C) averaged from 21 August to 20 September, 2012, along the 150˚E meridian
Anomalies are deviations from the 1981 – 2010 average.

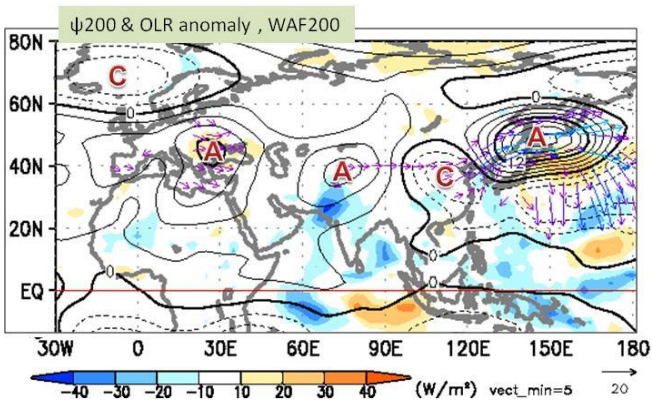

Figure 25 200-hPa stream function anomalies (contours), 200-hPa wave activity flux (vectors; unit: m^2/s^2), and outgoing longwave radiation (OLR) anomalies averaged from 21 August to 20 September, 2012
"A" and "C" indicate the centers of anticyclonic and cyclonic circulation anomalies, respectively. The contour interval is 3 × 10^6 m^2/s. Negative (cold color) and positive (warm color) OLR anomalies (unit: W/m^2) show enhanced and suppressed convection, respectively. Anomalies are deviations from the 1981 – 2010 average. The wave activity flux is calculated after Takaya and Nakamura (2001).

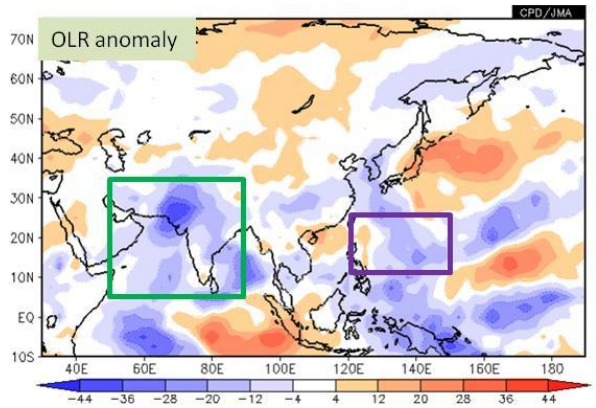

Figure 26 OLR anomalies averaged from 21 August to 20 September, 2012
The green and purple rectangles indicate the area around South Asia (5˚N – 35˚N, 50˚E – 90˚E) and the area northeast of the Philippines (10˚N – 25˚N, 120˚E –150˚E), respectively. Anomalies are deviations from the 1981 – 2010 average.

In late August and mid-September 2012, convective activity was enhanced northeast of the Philippines (Figure 26); several typhoons formed in the area, moving northward over Okinawa (southwestern Japan) and the South China Sea (Figure 28). According to statistical analysis, wave trains tend to appear in the area from the Philippines to Japan and the northern Pacific in association with the variability of convective activity northeast of the Philippines from late August to mid-September (Figure 29). This teleconnection formation is called the Pacific-Japan (PJ) pattern (Nitta 1986; 1987). The outcomes of statistical analysis and research performed to date indicate that active convection northeast of the Philippines and typhoons contributed to the strength of the Pacific High over northern and eastern Japan.

The possible primary factors contributing to Japan's hot late-summer conditions are summarized in Figure 30, but the related mechanisms have not yet been fully clarified.

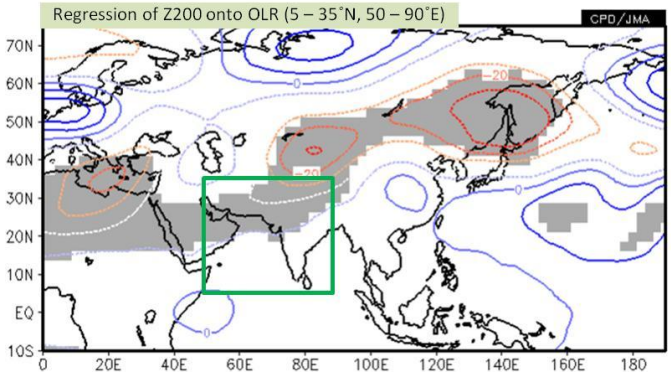

Figure 27 200-hPa geopotential height (contours; unit: m) regressed onto a time-series representation of area-averaged OLR values in and around South Asia (green rectangle: 5˚N – 35˚N, 50˚E – 90˚E) for the period from 21 August to 20 September, 2012

The contour interval is 5 m. The gray shading indicates a 95% confidence level. The base period for the statistical analysis is 1979 – 2011.

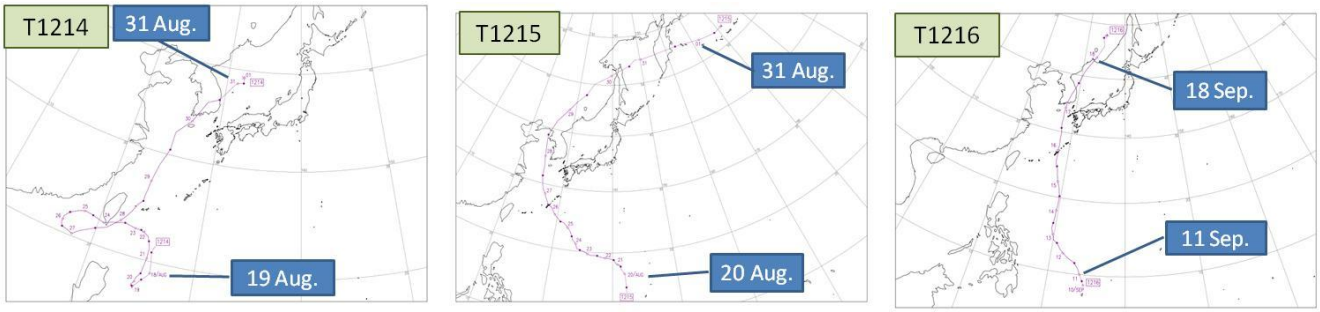

Figure 28 Typhoons forming from late August to mid-September 2012

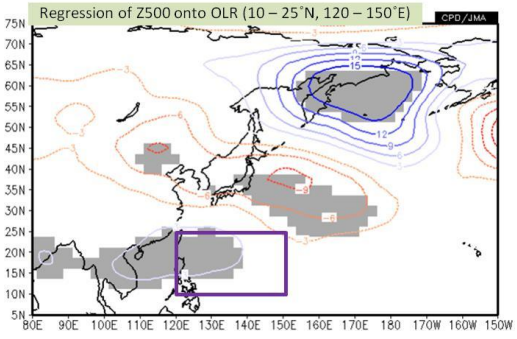

Figure 29 500-hPa geopotential height (contours; unit: m) regressed onto a time-series representation of area-averaged OLR values for the area northeast of the Philippines (purple rectangle: 10˚N – 25˚N, 120˚E – 150˚E) covering the period from 21 August to 20 September

The contour interval is 3 m. The gray shading indicates a 95% confidence level. The base period for the statistical analysis is 1979 – 2011.

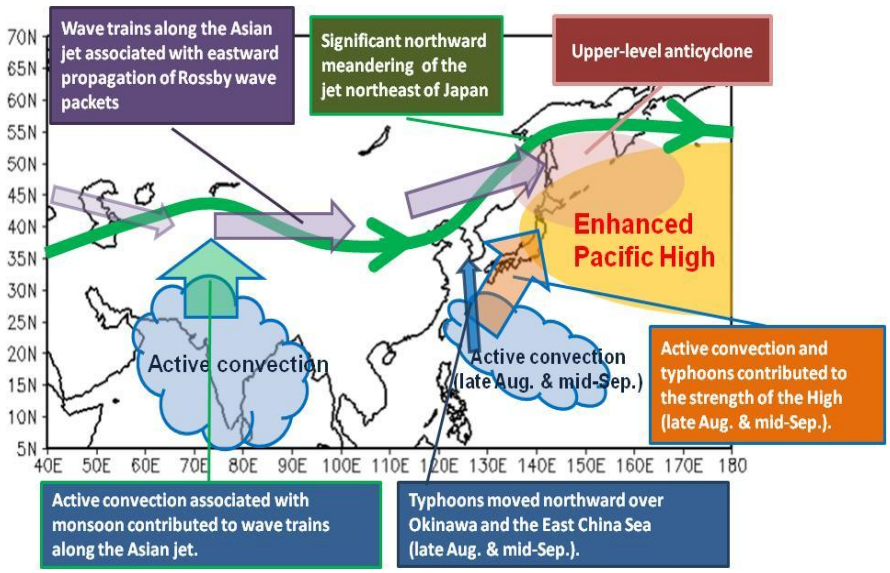

Figure 30 Primary factors contributing to the hot late-summer conditions of 2012 in northern and eastern Japan

3. Sea surface temperatures around northern Japan

Sea surface temperatures (SSTs) around northern Japan were significantly higher than normal (i.e., the 1981 – 2010 average) from late August to mid-September 2012 (Figure 31). The value of 10-day mean SSTs averaged for the area around Hokkaido (the white rectangle in Figure 31) for mid-September 2012 was 22.5˚C (preliminary), which was 4.6˚C above normal (Table 4) and exceeded the previous record of 21.4˚C set in late August 2010 for all 10-day periods of the year since 1985. In the normal, SSTs in the area reach annual maximum levels in August and September. The values of area-averaged SSTs for the two consecutive 10-day periods of early and mid-September 2012 were the highest on record for the respective periods of the year since 1985 (Table 4; Figure 32).

In the seas around Hokkaido, surface seawater was warmer than normal due to predominant sunny conditions (i.e., above-normal amounts of solar radiation) associated with the enhanced North Pacific High that caused record-breaking high temperatures in northern Japan. In addition, near-surface seawater was less mixed with cold seawater below it by surface winds, and ocean heat accumulated between the surface and just above 10 m in depth due to calm conditions associated with the enhanced Pacific High (Figure 33). The record-high SSTs observed around Hokkaido can be attributed to these factors relating to the enhanced North Pacific High east of Japan.

(1-2: Shotaro Tanaka, Climate Prediction Division,
3: Satoshi Matsumoto: Office of Marine Prediction)

References

Enomoto, T., B. J. Hoskins, and Y. Matsuda, 2003: The formation mechanism of the Bonin high in August, *Quart J. Roy. Meteor. Soc.*, **587**, 157-178.

Enomoto, T., 2004: Interannual variability of the Bonin high associated with the propagation of Rossby waves along the Asian jet. J. Meteor. Soc. Japan, **82**, 1019-1034.

Hoskins, B., M. E. McIntyre, and A. W. Robertson, 1985: On the use and significance of isentropic potential vorticity maps, *Quart J. Roy. Meteor. Soc.*, **111**, 877-946.

Nitta, T., 1986: Long-term variations of cloud amount in the western Pacific region. *J. Meteor. Soc. Japan*, **64**, 373-390.

Nitta, T., 1987: Convective activities in the tropical western Pacific and their impact on the Northern Hemisphere summer circulation. *J. Meteor. Soc. Japan*, **65**, 373-390.

Takaya, K., and H. Nakamura, 2001: A formulation of a phase-independent wave-activity flux for stationary and migratory quasigeostrophic eddies on a zonally varying basic flow. *J. Atom. Sci.*, **58**, 608 – 627.

Table 4 Record-high (preliminary) 10-day mean SSTs (unit: ˚C) averaged over the area around Hokkaido in northern Japan for early and mid-September

The SST values for September 2012 are preliminary. Collection of statistical records began in 1985, since when SST statistics have been based on satellite observations in addition to ship observations. Anomalies are deviations from the 1981 – 2010 average. The area for the average is the white rectangle shown in Figure 31.

Seas around Hokkaido	Area-averaged SSTs	Anomalies	Previous record high
1 – 10 September	21.8	+3.3	21.1 (2010)
11 – 20 September	22.5	+4.6	20.1 (1999)

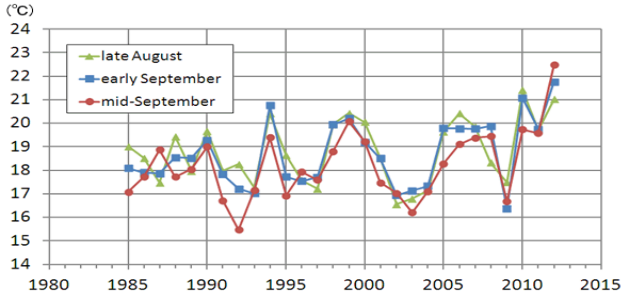

Figure 32 Interannual variability of 10-day mean SSTs averaged over the area around Hokkaido (white rectangle shown in Figure 31) for late August (green line), early September (blue line) and mid-September (red line) from 1985 to 2012

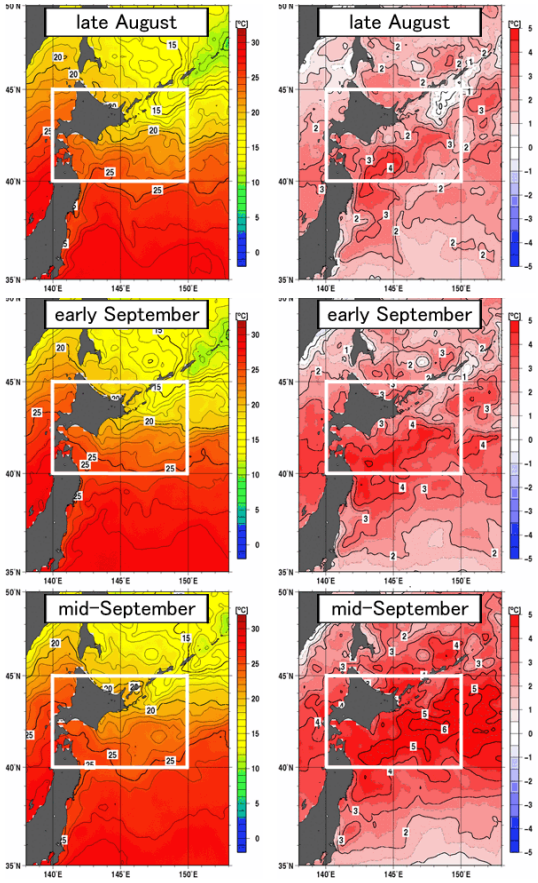

Figure 31 10-day mean SSTs (left) and anomalies (right) for late August (top), early September (middle) and mid-September 2012 (bottom)

Anomalies are deviations from the 1981 – 2010 average, and the unit for SSTs and anomalies is ˚C. The white rectangle indicates the target area around Hokkaido.

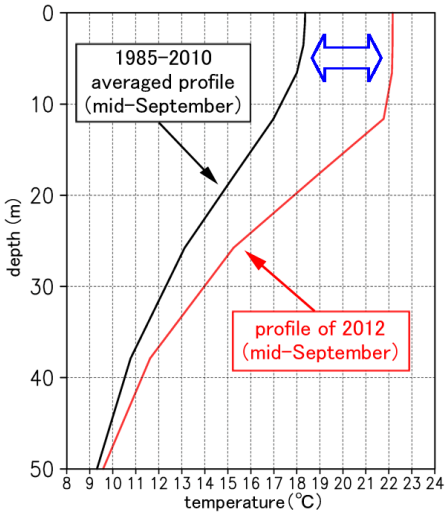

Figure 33 Temperature profile for seawater between the surface and a depth of 50 m averaged over the area around Hokkaido (white rectangle shown in Figure 31) for mid-September of 2012 (red line) and the 1985 – 2010 average (black line)

Deviations from the 1985 – 2010 average were significant between the surface and just above 10 m in depth, and were small at 50 m in depth.

Sea Ice in the Arctic Ocean for the 2012 Summer Season

The sea ice extent in the Arctic Ocean for the 2012 summer season was the smallest since 1979.

On 5 March, 2012, the sea ice extent in the Arctic Ocean reached its annual maximum of 15.48 million square kilometers (nearly normal based on the 1981 – 2010 average; Figure 34) before decreasing at a nearly normal rate until the end of May. However, the rate of decrease in the Arctic Ocean has been rapid since early June, meaning that the sea ice extent there has been at or close to its minimum since mid-June. The rate of decrease is usually slow in August, but was rapid in August 2012.

On 19 August, the sea ice extent was below 4.31 million square kilometers, which was the second smallest recorded in 2007 since 1979, and reached 3.42 million square kilometers on 13 September.

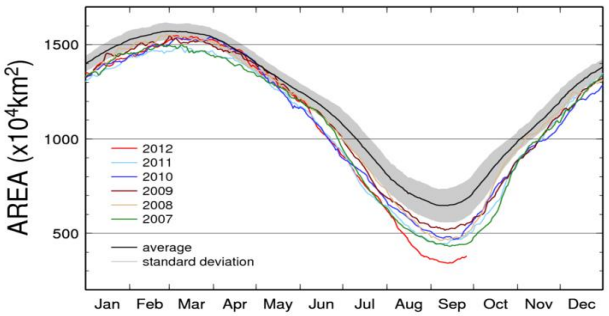

Figure 34 Time-series representation of daily sea ice extents in the Arctic Ocean from 1 January 2007 to 25 September 2012 and the normal (i.e., the 1981 – 2010 average)

Annual minimum sea ice extent in the Arctic Ocean

When the sea ice extent in the Arctic Ocean reached its minimum, extents around the Canadian Archipelago, the Beaufort Sea, the Laptev Sea and the Kara Sea were considerably reduced. This made the ice-free area north of the North American continent and the Eurasian continent larger than it was in September 2007 (Figure 35).

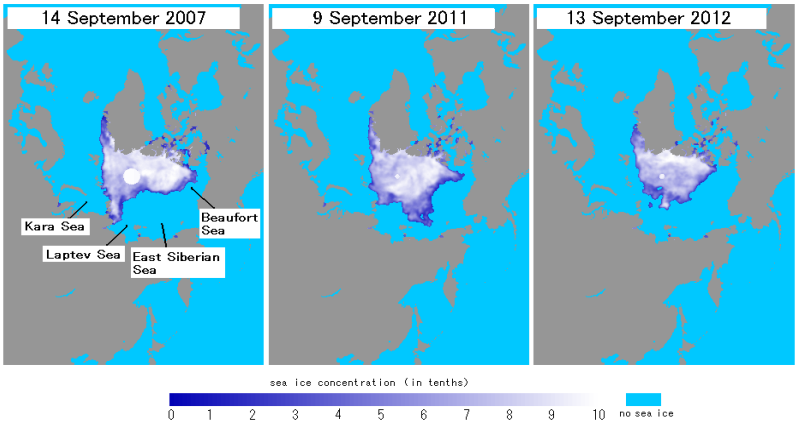

Figure 35 Annual minimum sea ice extents in the Arctic Ocean
Annual minimum sea ice extents for 2007 (left), 2011 (center) and 2012 (right)

Summer weather conditions over the Arctic Ocean and factors behind the remarkable decrease in the sea ice extent

The pressure pattern from June to August of 2012 featured a high-pressure area centered over Greenland and a low-pressure area near Siberia. Contributing to the remarkable decrease of the sea ice extent were higher-than-normal air temperatures over the Canadian Archipelago and the Beaufort Sea due to an inflow of warm southerly winds on the eastern side of the low-pressure area near Siberia. An early-August area of developed low pressure centered over the Arctic Ocean that caused sea ice to melt rapidly is considered to be another factor behind the remarkable decrease. The pressure patterns observed from June to August of 2007 (when the second-smallest sea ice extent on record was observed) and from June to July of 2011 (when the third-smallest was observed), which featured a high-pressure area centered near the Beaufort Sea and a low-pressure area centered over Siberia, differed from that seen from June to August of 2012. The factors contributing to the decreases in the sea ice extent in 2007 and 2011 were: (1) warm winds flowing from the Bering Sea to the sea along Siberia; (2) westward movement of sea ice north of Siberia; and (3) sea ice flow out to the Atlantic Ocean via the sea east of Greenland (Figure 36). A long-term downward trend for the sea ice extent in the Arctic Ocean is seen (Figure 37). The factors causing the smallest sea ice extent for summer 2012 are considered to be the long-term trend of decrease and prevailing weather conditions.

(Keiji Hamada, Office of Marine Prediction)

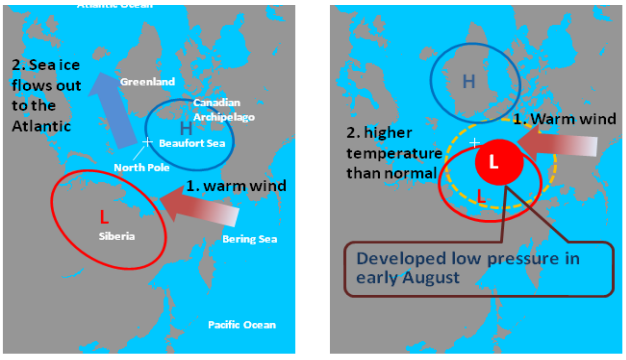

Figure 36 Schematic representation of summer weather patterns over the Arctic Ocean
Left: weather patterns for 2007 and 2011; right: weather patterns for 2012

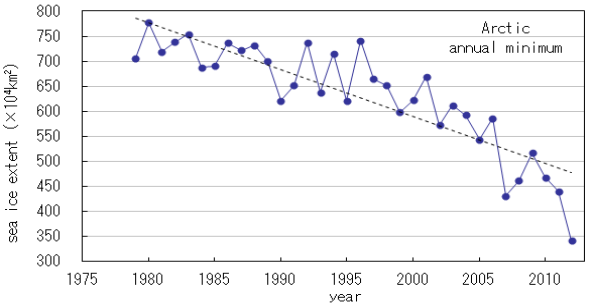

Figure 37 Interannual variations of annual minimum sea ice extent in the Arctic Ocean
The blue line indicates interannual variations of the annual minimum sea ice extent from 1979 to 2012. The dashed line indicates the trend for 1979 to 2012.

Status of the Antarctic Ozone Hole in 2012

The ozone hole was at its smallest since the 1990s.

The Antarctic ozone hole in 2012 was the smallest in terms of its annual maximum area since the 1990s (see the upper right panel in Figure 38) according to JMA's analysis based on data from National Aeronautics and Space Administration (NASA) satellites. Higher temperatures in the lower stratosphere contributed to the smaller coverage of the hole during Antarctic spring. However, the hole is still large compared to its size in the early 1980s, which is consistent with the high levels of ozone-depleting substances in the Antarctic atmosphere.

Over the last 30 years, the Antarctic ozone hole has appeared every year in Austral spring with a peak in September or early October. In 2012, it formed in mid-August and expanded rapidly from late August to early September, reaching its maximum size for the year on 22 September. At this time it covered 20.8 million square kilometers (upper left panel), which is 1.5 times the area of the Antarctic Continent. The gray shading in the bottom panels indicates the progress of the hole's development and intensity this year.

The ozone layer acts as a shield against ultraviolet radiation, which can cause skin cancer. The ozone hole first appeared in the early 1980s and reached its maximum size of 29.6 million square kilometers in 2000. Although this year's was the smallest since the 1990s, the amount of ozone in the Antarctic region is expected to return to pre-1980 levels in the late 21st century according to WMO/UNEP Scientific Assessment of Ozone Depletion: 2010. Close observation of the ozone layer on a global scale (including that over the Antarctic region) remains important.

(Hiroaki Naoe, Ozone Layer Monitoring Office, Atmospheric Environment Division)

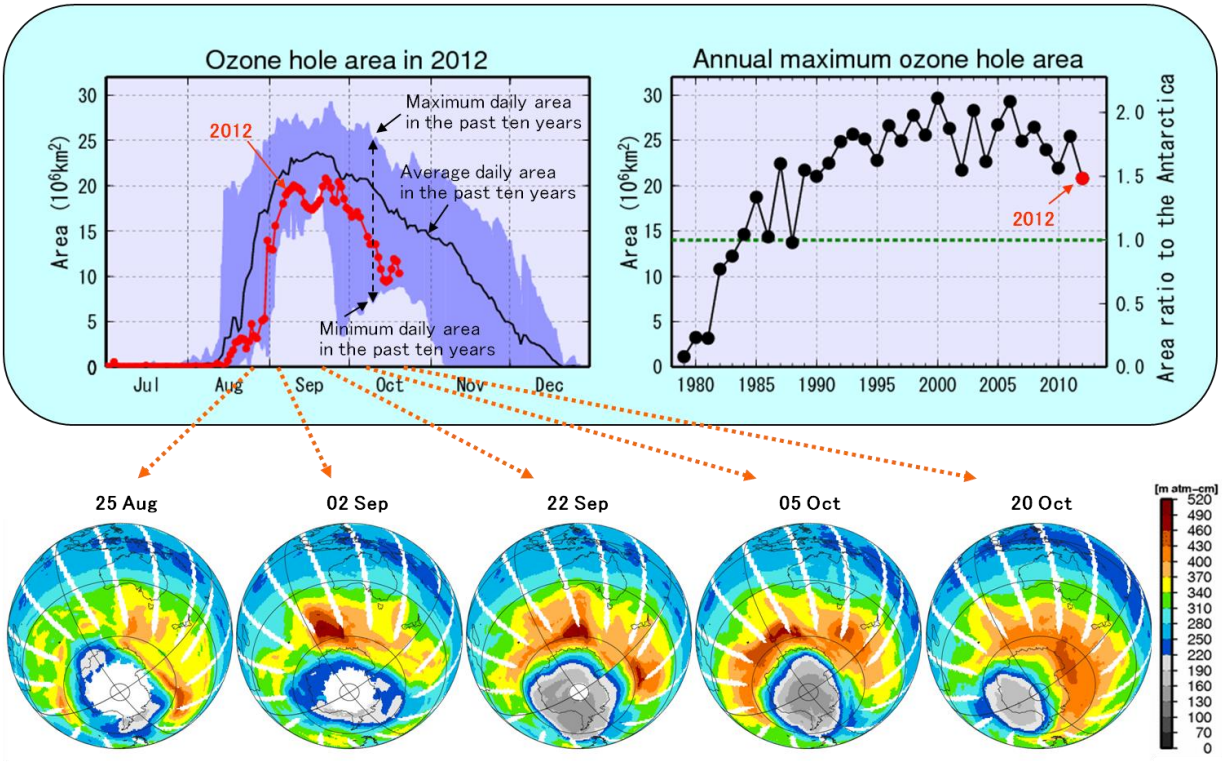

Figure 38
Antarctic ozone hole characteristics
Upper left: Time-series representation of the daily ozone-hole area for 2012 (red line) and the 2002–2011 average (black line). The blue shading area represents the range of daily minima and daily maxima over the past 10 years. Upper right: Interannual variability in the annual maximum ozone-hole area. Bottom: Snapshots of total column ozone distribution on selected days in 2012; the ozone hole is shown in gray. These panels are based on data from NASA satellite sensors of the total ozone mapping spectrometer (TOMS) and ozone monitoring instrument (OMI).

Any comments or inquiry on this newsletter and/or the TCC website would be much appreciated. Please e-mail to tcc@met.kishou.go.jp.
(Editors: Teruko Manabe, Ryuji Yamada and Kenji Yoshida)

Tokyo Climate Center (TCC), Climate Prediction Division, JMA
Address: 1-3-4 Otemachi, Chiyoda-ku, Tokyo 100-8122, Japan
TCC Website: http://ds.data.jma.go.jp/tcc/tcc/index.html